High Pressure Research
An International Journal
Publication details, including instructions for authors and subscription information:
http://www.informaworld.com/smpp/title~content=t713679167

The high-pressure phase diagram of ammonia dihydrate

To cite this Article: Fortes, A. D., Wood, I. G., Alfredsson, M., Vočadlo, L., Knight, K. S., Marshall, W. G., Tucker, M. G. and Fernandez-Alonso, F. , 'The high-pressure phase diagram of ammonia dihydrate', High Pressure Research, 27:2, 201 - 212
To link to this article: DOI: 10.1080/08957950701265029
URL: http://dx.doi.org/10.1080/08957950701265029

High Pressure Research
Vol. 27, No. 2, June 2007, 201–212

Taylor & Francis
Taylor & Francis Group

The high-pressure phase diagram of ammonia dihydrate

A. D. FORTES*†, I. G. WOOD†, M. ALFREDSSON†, L. VOČADLO†, K. S. KNIGHT‡, W. G. MARSHALL‡, M. G. TUCKER‡ and F. FERNANDEZ-ALONSO‡

†Department of Earth Sciences, University College London, Gower Street, London WC1E 6BT, United Kingdom
‡ISIS Facility, Rutherford Appleton Laboratory, Chilton, Didcot, Oxfordshire OX11 0QX, United Kingdom

(Received 30 November 2006; revised 06 February 2007; in final form 7 February 2007)

We have investigated the P–T phase diagram of ammonia dihydrate (ADH), $ND3 \cdot 2D_2O$, using powder neutron diffraction methods over the range 0–9 GPa, 170–300 K. In addition to the ambient pressure phase, ADH I, we have identified three high-pressure phases, ADH II, III, and IV, each of which has been reproduced in at least three separate experiments. Another, apparently body-centred-cubic, phase of ADH has been observed on a single occasion above 6 GPa at 170 K. The existence of a dehydration boundary has been confirmed where, upon compression or warming, ADH IV decomposes to a high-pressure ice phase (ice VII or VIII) and a high-pressure phase of ammonia monohydrate (AMH V or VI).

Keywords: Ammonia dihydrate; Neutron diffraction; Polymorphism

1. Introduction

The ammonia–water system is of considerable interest to physical chemistry for its mixture of homonuclear and heteronuclear hydrogen bonds. The end member phases, and the stoichiometric hydrates, ammonia dihydrate ($NH_3 \cdot 2H_2O$, ADH), ammonia monohydrate ($NH_3 \cdot H_2O$, AMH), and ammonia hemihydrate ($2NH_3 \cdot H_2O$, AHH), are therefore model systems for understanding the behaviour of bonds which occur in far more complex molecules, *e.g.*, DNA. Moreover, ADH is of interest in the field of planetary science, since astronomical observations and cosmochemical models indicate that ammonia may be a significant component of outer solar system ices; the predicted ammonia abundances (5–10 wt.%) should result in the formation of ADH + ice [1, 2]. The pressure melting curve, and the expected polymorphism of ADH have implications for the internal structure of large icy moons, leading to phase layering and the possible persistence of a deep subsurface oceans [3, 4]. Since the rich polymorphism and physical properties of water ices continue to shed new light on the behaviour of the homonuclear hydrogen bond between water molecules in the solid state [5], we can expect to learn more from studying the phase behaviour and physical properties of ammonia hydrates under high pressures.

*Corresponding author. Email: andrew.fortes@ucl.ac.uk

High Pressure Research
ISSN 0895-7959 print/ISSN 1477-2299 online © 2007 Taylor & Francis
http://www.tandf.co.uk/journals
DOI: 10.1080/08957950701265029

The behaviour of ADH at high pressure has been investigated by a number of groups [6–17]; for the most part these studies focused on establishing the high-pressure melting curve. Hogenboom *et al.* [15] were the first to detect a new high-pressure phase – ammonia dihydrate II (ADH II) – which their dilatometry measurements showed to be stable above ∼400 MPa at 170 K. Shortly afterwards, a powder neutron diffraction pattern of ADH II was reported by Nelmes *et al.* [18] with data acquired at 530 MPa and 170 K, using a gas pressure cell on the POLARIS diffractometer at ISIS. In contrast, Raman and optical studies of both ADH [10] and AMH [19] using diamond anvil cells (DACs) did not indicate the existence of any high-pressure polymorphs. However, AMH has since been shown to exhibit a range of high-pressure polymorphs [20], and photomicrographs of high-pressure ADH crystals [10] do not display the cubic symmetry of the low-pressure phase.

This article describes a series of experimental investigations, carried out using powder neutron diffraction, of the high-pressure behaviour of ADH.

2. Experimental method

2.1 *Sample preparation and loading*

Samples were prepared by condensing ND_3 gas into an evacuated glass bulb cooled to ∼220 K in a dry ice–acetone bath. The bulb was weighed and the contents diluted to the appropriate stoichiometry (33.3 mol.% ND_3) with D_2O. The solution was warmed, shaken and then stored in a refrigerator until use. In all studies to date, samples have been loaded into their respective containers as liquids. While it is possible to flash-freeze the liquid in nitrogen and then grind the resulting glass, there are practical difficulties (particularly with the gas-cells) in loading the powder and then forming a good pressure seal. $ND_3 \cdot 2D_2O$ liquid has therefore been loaded with tufts of silica wool (typically ∼0.1 g) to promote nucleation of a suitably random polycrystalline mass. In the ambient pressure investigations, the specimen was contained in an aluminium 'slab-can' (sample volume ∼5 cm^3). High-pressure neutron diffraction investigations in the range of 0–550 MPa were carried out in aluminium or TiZr gas cells (sample volume ∼2 cm^3) using helium as the pressure transmitting medium. Higher-pressure investigations in the range 0.5–9 GPa were made using Paris-Edinburgh cells with the sample contained in encapsulated TiZr gaskets (sample volume ∼0.1 cm^3 [21]); see Bailey [22] for a review of high-pressure sample environments in neutron scattering.

Loading liquid ADH near room temperature results in ammonia boiling out of solution; consequently, solid specimens are found to contain ∼10 wt.% ice. Phase pure samples have been produced by loading samples in the ISIS cold room (air temperature −10°C) using a syringe cooled in a dry ice-acetone bath. Care must be taken in avoiding exposure of ADH liquid to CO_2, which results in precipitation of solid ammonium carbonate, or to certain metallic alloys: we have observed the formation of a blue copper–ammonia complex after using syringe needles with chrome-plated brass hubs, a phenomenon which has been reported elsewhere with saline solutions [23]. ADH solution decanted into a small glass bottle and dipped momentarily in liquid nitrogen yields a sufficiently viscous material to fill easily the encapsulated gaskets of the Paris-Edinburgh cell.

ADH is notoriously difficult to crystallise, as a result of the high viscosity of the liquid phase near the melting point. It is customary to flash-freeze such materials to form an amorphous solid using liquid nitrogen and then warm through the glass transition temperature. However, in ADH, devitrification is very slow, so crystallisation is promoted by thermal cycling close to the melting point. In our experience, crystallisation at pressures of a few hundred megapascal in the gas cell has never proven successful, even with a protracted period of temperature cycling.

In the Paris-Edinburgh cell, we normally compress the liquid under a load of 12 tons (∼1 GPa) at room temperature, and then cool the cell by the simple expedient of spraying liquid nitrogen over the cell body. As the sample cools and contracts, the pressure falls, dropping to 600 MPa as the freezing point is reached near 200 K; this typically takes several hours. Crystallisation under these conditions occurs only with significant undercooling or super-pression, but is quite rapid once begun.

2.2 *Data collection*

Powder neutron diffraction studies were carried out at the ISIS neutron spallation source (Rutherford Appleton Laboratory, Chilton, UK). Ambient pressure, low-temperature work, and high-pressure studies using aluminium and TiZr gas pressure vessels (rated to 450 and 550 MPa respectively), were carried out using the HRPD and OSIRIS instruments. HRPD is the highest resolution powder diffractometer in the world, with an almost constant resolution, $\Delta d/d = 10^{-4}$ in the backscattering detectors ($2\theta = 168°$), across a range of d-spacings from ∼0.5 to 3.5 Å [24]. With an appropriate chopper phasing HRPD can be used to measure d-spacings as large as ∼8 Å, but the low-neutron flux from the methane moderator at longer wavelengths, combined with the halved neutron pulse frequency (to avoid frame overlap), is a limiting factor in this time-of-flight window. To make longer d-spacing measurements with the gas pressure cells, we used the OSIRIS diffractometer [25]; OSIRIS views a hydrogen moderator from the end of a 35 m beamline, which allows the user to examine d-spacings, in principle, as large as ∼30 Å with a resolution in backscattering ($2\theta = 157$–$169°$) that compares very favourably to the 90° detector banks on HRPD. Higher pressures were achieved using the Paris-Edinburgh opposed anvil press on the PEARL beamline's HiPr diffractometer. Using this cell, one can readily study the pressure range from 0 to 9 GPa at temperatures as low as ∼100 K, measuring d-spacings from ∼0.7 to 4 Å with a resolution of $\Delta d/d = 8 \times 10^{-3}$. Pressure determination in the Paris-Edinburgh cell was achieved using an internal calibrant, since the anvil geometry prevents a simple calculation of the pressure in the sample space from the applied load. Lead is a suitable pressure marker as it is relatively compressible, and unlikely to react with the sample. The Pb equation of state used for this work is given in the appendix. We have found that crystallisation is markedly quicker when the lead pressure calibrant is included than when it is not present.

3. The high-pressure phase diagram of ADH

The phase boundaries in the 0–1 GPa range are shown in figure 1a and b, and in the 0–9 GPa range in figure 2. These diagrams (in particular the melting curves) are drawn largely from the literature (section 1). The complexity of the liquidus surface, as ADH apparently switches from incongruent to congruent melting and back again repeatedly, may be better understood by reference to figure 1b, which shows a further synthesis of literature data in P–T–X space. Some disagreement in the position of the peritectic between 0.5 and 1.0 GPa is discussed in section 4. The subsolidus phase boundaries are determined from this work and should be considered highly speculative until such time as the phase diagram can be mapped more finely. The dehydration line in figure 2 is taken from the DAC observations of Boone [10], and since our observations agree so well, it stands. Figure 3 shows the highest quality diffraction data collected so far from the three reproducible single-phase high-pressure polymorphs of ADH discussed below.

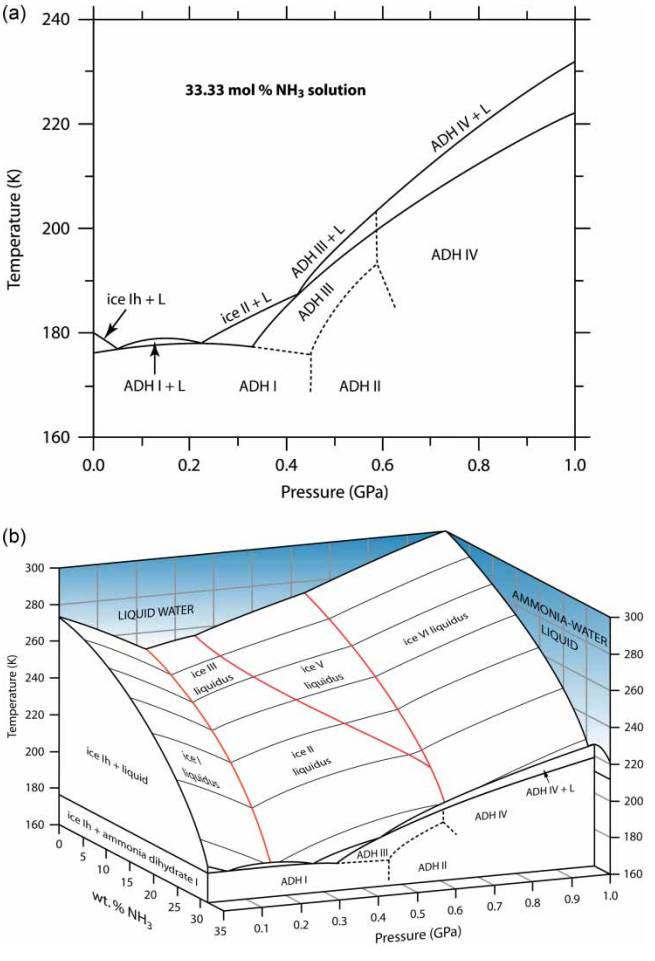

Figure 1. (a) The low-pressure (0–1 GPa) region of the ADH phase diagram: liquidus phase boundaries are adapted from refs. [10, pp. 129–133, 15], and the dashed lines represent phase boundaries inferred from our observations; (b) The P-T-X diagram at the water-rich end of the NH_3-H_2O binary system over the same pressure region as (a).

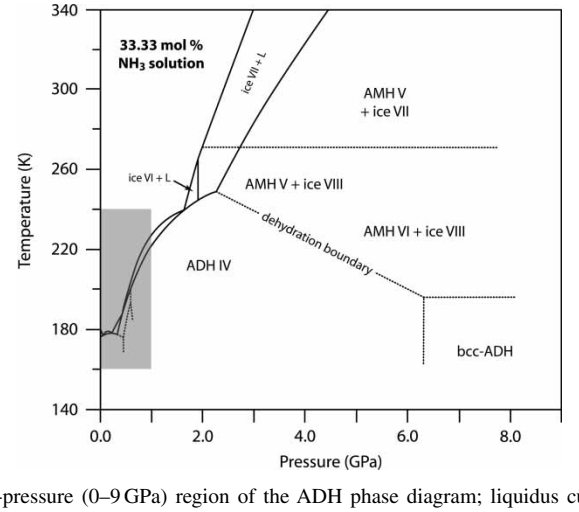

Figure 2. The higher-pressure (0–9 GPa) region of the ADH phase diagram; liquidus curves are redrawn after refs. [10, pp. 117, 120, 15]. The grey box indicates the P–T range covered in figure 1a.

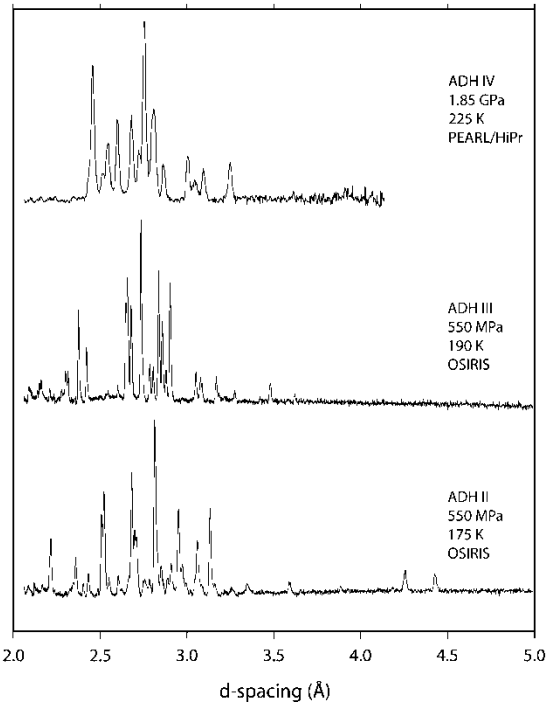

Figure 3. The best neutron diffraction patterns of ADH phases II, III, and IV collected to date.

3.1 *The ambient pressure phase, ADH I*

ADH I was first identified by Rollet and Vuillard [26]; at ambient pressure it melts incongruently at 176.13 K [27]. The first structural study combined X-ray diffraction and infrared spectroscopy, concluding that ADH I was probably orientationally ordered in space group $P2_12_12_1$ [28], in agreement with the low-temperature heat capacity measurements [27]. However, powder neutron diffraction showed that ADH I is cubic, space group $P2_13$ with $Z = 4$ and $a = 7.1278(8)$ Å at 150 K [20, 29]. Fortes *et al.* [30] carried out a first principles computational study of ADH I, and a powder neutron diffraction study [31], measuring the thermal expansivity from 4 to 175 K at ambient pressure, and the incompressibility from 0 to 450 MPa at 175 K.

3.2 *Ammonia dihydrate phase II* (*ADH II*)

We have formed single-phase ADH II in four independent experiments by compression of ADH I above 470 MPa at 175 K. We have also made a mixture of ADH II and another high-pressure polymorph, ADH III (section 3.3), by melting ADH I at 460 MPa, 179 K. Our diffraction patterns, collected both on HRPD and OSIRIS (figure 4) are in substantial agreement with the diffraction pattern observed on the POLARIS diffractometer, also at ISIS, by Nelmes *et al.* [18]. As shown in figure 4, however, there are some significant differences in the relative intensities of certain Bragg reflexions. There are a number of possible explanations for these additional strong 'satellite' reflexions: (1) the specimens are not a single phase; (2) the specimens exhibit varying degrees of preferred orientation; and (3) these are super-lattice reflexions which represent differing amounts of hydrogen-bond ordering. If, in the first instance, there is more than one phase present, there are only a limited range of options. The sample may

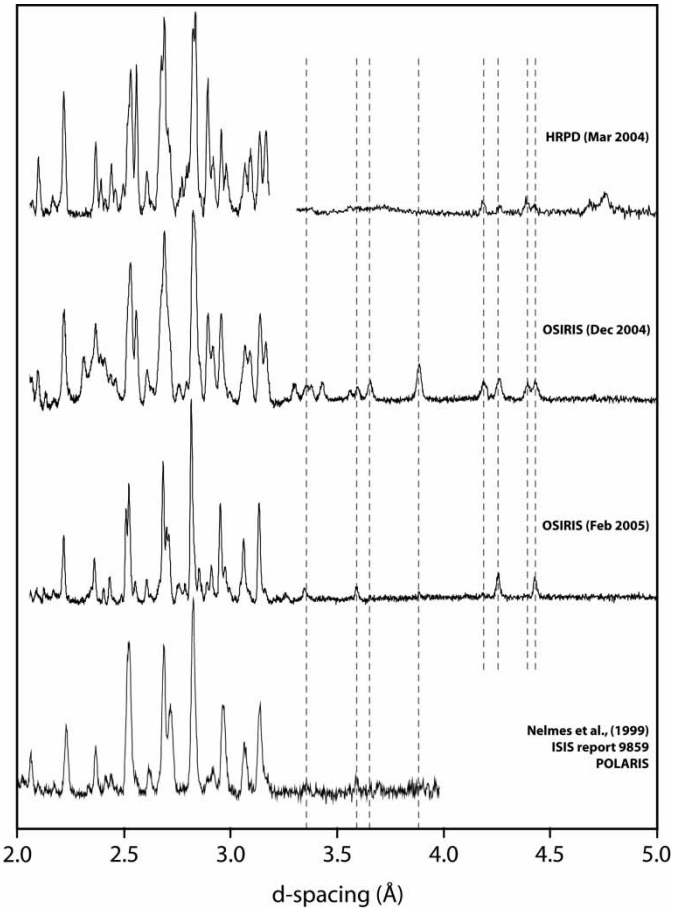

Figure 4. Diffraction patterns of ADH II acquired under nearly identical conditions of pressure and temperature. The uppermost pattern, from the HRPD 90° detector banks, was counted in two separate time-of-flight windows so, following normalisation, there is a small gap near 3.25 Å. Due to longer counting times in the February 2005 OSIRIS experiment, we present data at 5% resolution (*i.e.*, using the 5% of detectors at the highest Bragg angle), whereas the December 2004 OSIRIS data are shown at 100% resolution (*i.e.*, using the full range of detector solid angles).

have exsolved into AMH + ice: however, none of the Bragg peaks match the known phases of AMH or water ice. Moreover, these samples undergo a solid-state transformation to ADH III (see below), which we are more confident is a single phase. The specimen might consist of two discrete ADH phases, but it would be a remarkable coincidence if the Bragg peaks of one occurred as satellites of the other unless both had very similar structures. In which case it is possible that the sample consists of discrete regions of proton-ordered and proton-disordered ADH II, and that these have slightly different unit cell dimensions, although proton ordering usually has an insignificant effect on cell parameters.

The sample examined by Nelmes *et al.* [18] was not textured (J.S. Loveday, pers. comm.), and none of the other phases we have examined show evidence of significant preferred orientation. The texture would need to be considerable in order to have an effect of the observed magnitude, but we cannot rule it out at present.

We consider it most probable that the satellites are super-lattice reflections. Low-index superlattice reflexions typically occur midway between sub-lattice reflexions; for the case of one axis being doubled in length, higher order Miller indices can be found as close satellites, either on the high or low d-spacing side of existing sub-lattice peaks, as we observe here. This suggests

a relatively large supercell, perhaps twice the size of the ADH I unit cell (*i.e.*, with $Z = 8$). The strength of the purported super-lattice reflexions (from the bottom up in figure 4) may be due to increasing hydrogen-bond ordering in the structure, which might in turn depend on the thermal history of the sample.

In our studies, ADH II has been recovered to ambient pressure after cooling to 150 K, although the resulting diffraction pattern exhibited severe strain broadening.

Hogenboom *et al.* [15] observed the ADH I–II transition at temperatures from 150 to 175 K. However, the slightly negative sign of $\mathrm{d}T/\mathrm{d}P$ for their phase boundary is consistent with similar work on the water ice phase diagram *e.g.*, ref. [32] in which increasingly sluggish kinetics below 200 K push the observed transition to higher pressures as the temperature is reduced; in other words, the observed phase boundary is probably not the *equilibrium* phase boundary. By analogy with ice, where the only significant entropy differences between phases are due to proton ordering, we would expect the ADH I–II slope to be vertical if ADH II is orientationally disordered, and have a positive $\mathrm{d}T/\mathrm{d}P$ slope if it is ordered.

Due to the high-pressure ceiling of the TiZr pressure cell (550 MPa), we have not been able to determine the upper stability limit of ADH II, and we have not conclusively formed ADH II in work with the Paris-Edinburgh cell (section 3.5). It is worth noting that Loveday and Nelmes [29] reported pressure amorphisation of ADH I in the Paris-Edinburgh cell when compressed (at an unreported temperature) under a load of 30 tons (∼2.5 GPa), which persisted up to 70 tons (∼7 GPa).

3.3 *Ammonia dihydrate phase III* (*ADH III*)

Warming of ADH II at 550 MPa results in a phase transformation at 190 K to ADH III (figure 3); this phase has been seen in three independent experiments, in each case with highly reproducible intensities, indicative of a lack of significant preferred orientation. ADH III melts *congruently* at 196 K at 550 MPa (figure 1a), and can be cooled metastably into the stability field of ADH II. We have collected diffraction patterns from ADH III down to 150 K, although it probably can persist metastably at lower temperatures and may, like ADH II, be recoverable to ambient pressure. ADH III has also been observed to form with ADH II following the melting of ADH I at 460 MPa, 179 K. Upon cooling to 175 K, ADH III nucleated and began to grow in under 10 min, whereas ADH II was not seen to nucleate until over an hour later; crystallisation was complete in ∼2 h. This gives us reason to suspect that ADH III is the liquidus phase from at least 450–550 MPa, although we have not yet succeeded in crystallising it directly from the liquid in this pressure range, even with temperature cycling. The high-pressure stability limit of ADH III has not been found experimentally, but cannot be much higher than 550 MPa since we have observed another high-pressure polymorph, ADH IV, to be the liquidus phase at ∼600 MPa.

3.4 *Ammonia dihydrate phase IV* (*ADH IV*)

ADH IV has been grown from the liquid phase in the region of 600 MPa, 200 K in six loadings of the Paris-Edinburgh cell using three distinct batches of ADH solution. ADH IV has been formed both with and without silica wool and lead in the gasket space, and has been observed co-existing with ice VI (in a sample containing the blue Cu-NH_3 complex mentioned in section 2.1). ADH IV has also been made by decompression of the high-pressure phase described in section 3.5. In all cases, the diffraction patterns (*e.g.*, figure 3) exhibit highly reproducible intensities, indicative of a well-randomised polycrystalline mass. ADH IV has the largest stability field of any high-pressure ADH phase yet investigated (figure 2) suggesting that it

has a relatively robust structure. We suspect that ADH IV is the liquidus phase from 0.6 to 2.0 GPa. A sample of ADH IV warmed to 240 K at 1.85 GPa underwent partial congruent melting; rapid cooling before melting was complete resulted in complete recrystallisation to phase IV. Note that Boone [10] observed incongruent melting to ice VI + liquid under these conditions (figure 2), and it is possible that the perdeuterated nature of our samples has influenced the loci of phase boundaries.

The behaviour of ADH IV under compression is described in section 3.6.

3.5 *BCC-ammonia dihydrate (ADH)*

During the first high-pressure study of ADH in the Paris-Edinburgh cell, a diffraction pattern was observed upon freezing of the liquid at 0.56 GPa, 170 K, which has not been observed since, and which does not appear to match any other phase seen before or since.[†] Compression of this phase at 170 K resulted in complete amorphisation at 2 GPa with a significant drop in load. Although some structure subsequently emerged in the diffraction pattern, the peaks were very broad, indicative perhaps of exceptionally small scattering domains. Continued compression ultimately resulted in the formation of a new phase at 6.3 GPa, 170 K. The new pattern is dominated by a single large Bragg reflexion from the sample near 2.31 Å (figure 5; nearly all of the other sharp peaks are from the pressure calibrant and anvils). The pattern is remarkable for its similarity to that of the high-pressure AMH VI phase [33]. AMH VI is a body-centred-cubic crystal which exhibits both substitutional and orientational disorder. It is possible that the sample has indeed exsolved (this certainly does occur at higher temperatures, see below) to form AMH VI, with the water expelled from the structure present as an amorphous solid since there is no sign of crystalline ice VIII. However, we consider this to be unlikely for the following reason. The bcc-cubic phase was observed at 6.3, 7.3, and 8.7 GPa (at 170 K), warmed to ∼190 K and decompressed to 4.5, 2.7, and 0.6 GPa at 190 K, whereupon the diffraction pattern of ADH IV was observed. It is most unlikely that, following exsolution, the two components could remix during rapid decompression. Hence, the bcc-cubic phase *must* be a single polymorph of ADH.

A model structure, based on that of AMH VI (space-group $Im\bar{3}m$, $Z = 1$) was fitted to the data at 8.75(15) GPa, 170 K using GSAS [34]. The $2a$ sites $(0, 0, 0)$ are assumed to be $2/3$ occupied by oxygen atoms and $1/3$ occupied by nitrogen atoms; deuterium atoms are distributed over two sites; 16f (0.1722, 0.1722, 0.1722) with an occupancy of 0.372, and 24 h (0.2109, 0.2109, 0) with an occupancy of 0.044. This yields the correct number of deuterium atoms per unit cell (seven), and mimics the directional distribution seen in AMH VI. This model provides an acceptable fit with a refined unit cell parameter, $a = 3.272(1)$ Å.

Several subsequent attempts to reproduce this polymorph by compression of phase IV have been thwarted by failure of the gaskets in the Paris-Edinburgh cell; it is unfortunate that, so far, this phase has only been seen once.

3.6 *The decomposition of ADH to AMH + ice*

Boone [10] reported optical studies of ADH in a DAC up to ∼7 GPa, including Raman spectra and images of crystals grown from the melt.[‡] Although no phase transitions were documented,

[†] We cannot rule out the possibility that this phase is ADH II; the presence of scattering from the anvils (tungsten carbide + nickel) and the lead pressure calibrant, as well as the significant neutron attenuation at d-spacings >3 Å prevent a definite identification.

[‡] This author also attempted to acquire X-ray diffraction patterns at high-pressure but was not successful (S.C. Boone, pers. comm.).

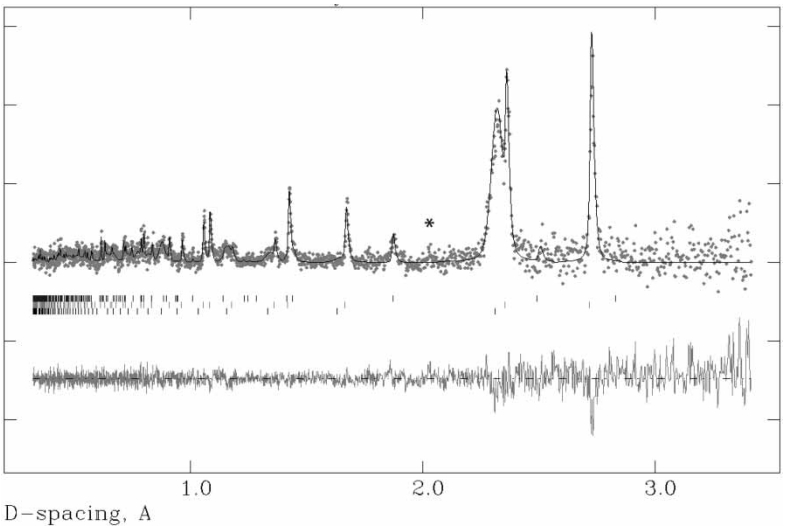

Figure 5. GSAS refinement of the bcc-ADH model at 8.75(15) GPa, 170 K. Data were collected for 6 h and fitted with a multiphase model, as described in section 3.5. The asterisk marks the strongest parasitic scattering from nickel, the anvil binding material, which was not included in the refinement. Tick marks are, from the top down; tungsten carbide, lead, and bcc-ADH.

a clear boundary was identified where ADH samples appeared to break down into a mixture of AMH + ice. Similarly, Johnson *et al.* [7] reported high-pressure phase separation yielding a myrmekitic intergrowth texture. In three separate experiments, we have observed this dehydration by isothermal compression, and on one occasion by isobaric warming.

ADH IV, when compressed above 6.5 GPa at 200 K, or warmed above 225 K at 4.4 GPa, transforms to a mixture of ice VIII and AMH VI: figure 6 shows the results of a multiphase Rietveld refinement of the data collected at 4.4 GPa, 230 K. Although the latter mixture was

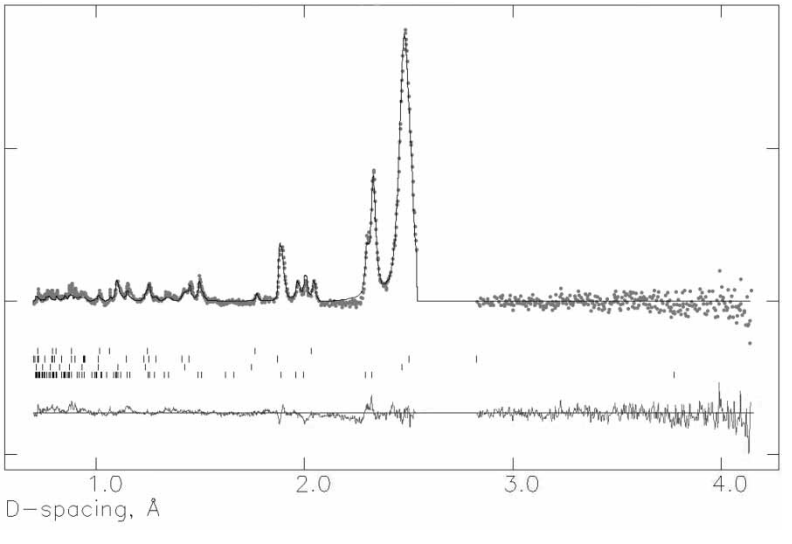

Figure 6. GSAS refinement of the AMH VI + ice VIII mixture at 4.4 GPa, 230 K. Data were collected for 12 h and fitted with a multiphase model; tick mark are, from the top down, nickel, tungsten carbide, AMH VI, and ice VIII. The excluded region near 2.75 Å covers a region where scattering from some residual ADH IV was present.

warmed to 283 K, no evidence of a transformation from ice VIII to ice VII was observed; cooling and unloading back through the dehydration boundary also did not lead to the formation of ADH, although this diffusion-limited reaction is probably kinetically inhibited at 170 K. Compression of ADH IV to 2.8 GPa at 230 K results in exsolution to yield ice VIII plus a phase we believe to be AMH V [20]. This transformation has been observed in two separate experiments at 230 K, once under a load of 32 tons and once at 34 tons, corresponding to pressures of 2.7–2.9 GPa. Further compression to 5.6 GPa and warming to room temperature produced a mixture of AMH V + ice VII.

4. Discussion

In spite of the excellent powder neutron diffraction data collected from ADH phases II, III, and IV, it has not proven possible to index the diffraction patterns satisfactorily. It might be argued that these 'phases' are in fact phase mixtures, which would certainly hinder indexing. However, for this to be true, we would need to have reproduced near identical mixtures in many experiments conducted over several years with fresh batches of initial liquid. Moreover, a phase transition of one component in the mixture would be expected to leave a residue of the second component: in all of the phase changes we observe, the supposed single-phase precursor transforms all at once. Finally, we have been able to recognise when mixtures *are* present, experiencing no difficulty in distinguishing ice phase VI, VII, and VIII in the presence of ADH and AMH.

Although we did not set out to examine the melting curve, we have acquired data which we believe can resolve a recent disagreement. Mousis *et al.* [17] investigated the peritectic melting point in the 0–1 GPa range, and obtained much higher values than had previously been published. Their work suggested a very steep rise in the peritectic at 500 MPa, from 185 to 230 K, with a plateau thereafter. These results were interpreted in terms of two new high-pressure phases, NP1 and NP2. We have, reproducibly, determined the melting point of ADH III at 550 MPa to be 196 K (the disappearance of Bragg peaks constitutes a robust observation of melting), and we have crystallised ADH IV at 600 MPa, 200 K in many experiments. Finally, we have melted ADH IV at 240 K, 1.85 GPa. These three observations agree very well with the data of Boone [10] and of Hogenboom *et al.* [15], but not with Mousis *et al.* [17]. Indeed, to agree with Mousis *et al.* [17] would imply that the melting point only increases by 10 K from 0.6 to 1.85 GPa, which is extremely difficult to countenance.

5. Summary

We have reported neutron powder diffraction data from four high-pressure polymorphs of ADH, all but one of which we have reproduced in at least three independent experiments. Diffraction patterns of ADH II, III, and IV have not been indexed. We have also directly observed the decomposition of one of those polymorphs (phase IV) to a mixture of AMH and ice, in agreement with earlier optical studies. It remains the case that we have not, with any certainty, observed any high-pressure phase of ADH both in the gas pressure cell *and* the Paris-Edinburgh cell. Ideally, we would wish to have a gas cell capable of extending our studies by a few hundred megapascal; this would allow us to observe the II–IV or III–IV transitions, and improve measurements of the melting point in that pressure range. The melting data reported here favour the melting measurements of Hogenboom *et al.* [15] over those of Mousis

et al. [17], findings which have consequences for thermal modelling of putative subsurface oceans inside Saturn's giant moon Titan.

Acknowledgements

The authors gratefully acknowledge the ISIS facility for beam time to conduct these experiments, and would like to thank the High-Pressure technical team for their patience and hard work; John Dreyer, Andy Church, Chris Goodway, Duncan Francis, and Jon Bones. The authors also acknowledge the assistance of Helen Brand, Peter Grindrod, and Katherine Joy. ADF is funded by a Fellowship from the Particle Physics and Astronomy Research Council (PPARC), grant number PPA/P/S/2003/00247. MA is funded by the Natural Environment Research Council (NERC), and LV is funded by the Royal Society.

References

[1] J.S. Kargel, Cryomagmatism in the Outer Solar System. PhD thesis, University of Arizona, Tucson (1990).
[2] J.S. Kargel, Icarus **100**(2) 556–574 (1992) (doi:10.1016/0019-1035(92)90118-Q).
[3] O. Grasset and C. Sotin, Icarus **123**(1) 101–112 (1996) (doi:10.1006/icar.1996.0144).
[4] O. Grasset, C. Sotin and F. Dechamps, Planet. Space. Sci. **48**(7–8) 617–636 (2000) (doi:10.1016/S0032-0633(00)00039-8).
[5] E.A. Zheligovskaya and G.G. Malenkov, Russ. Chem. Rev. **75**(1) 57–76 (2006) (doi:10.1070/RC2006v075n01ABEH001184).
[6] M.L. Johnson, A. Schwake and M. Nicol, Proc. Lunar Planet. Sci. **15** 405–406 (1984).
[7] M.L. Johnson, A. Schwake and M. Nicol, in *Ices in the Solar System*, edited by J. Klinger *et al.* (Reidel, Dordrecht, 1985), pp. 39–47.
[8] M.L. Johnson and M. Nicol, J. Geophys. Res. **92** 6339–6349 (1987).
[9] S.K. Croft, J.I. Lunine and J.S. Kargel, Icarus **73**(2) 279–293 (1988) (doi:10.1016/0019-1035(88)90098-X).
[10] S.C. Boone, PhD thesis, University of California, Los Angeles (1988).
[11] H.C. Cynn, S. Boone, A. Koumvakalis *et al.*, Proc. Lunar Planet. Sci. **19** 433–441 (1989).
[12] D.L. Hogenboom, J. Winebrake, G.J. Consolmagno *et al.*, Proc. Lunar Planet. Sci. **20** 420 (1989).
[13] D.L. Hogenboom and J.S. Kargel, Proc. Lunar Planet. Sci. **21** 522 (1990).
[14] S. Boone and M.E. Nicol, Proc. Lunar Planet. Sci. **21** 603–610 (1991).
[15] D.L. Hogenboom, J.S. Kargel, G.J. Consolmagno *et al.*, Icarus **128**(1) 171–180 (1997) (doi:10.1006/icar.1997.5705).
[16] J. Leliwa-Kopystínski, M. Maruyama and T. Nakajima, Icarus **159** 518–528 (2002)(doi:10.1006/icar.2002.6932).
[17] O. Mousis, J. Pargamin, O. Grasset *et al.*, Geophys. Res. Lett. **29**(24) article 2192 (2002) (doi:10.1029/2002GL015812).
[18] R.J. Nelmes, J.S. Loveday and M. Guthrie, Structural changes under pressure in ammonia dihydrate and ammonia hemihydrate. ISIS Experimental Report RB 9859, CCLRC Rutherford Appleton Laboratory (1999).
[19] A. Koumvakalis, High pressure study of ammonia monohydrate. PhD thesis, University of California, Los Angeles (1988).
[20] J.S. Loveday and R.J. Nelmes, High Press. Res. **24**(1) 45–55 (2004) (doi:10.1080/08957950410001661990).
[21] W.G. Marshall and D.J. Francis, J. Appl. Cryst. **35**(1) 122–125 (2002) (doi:10.1107/S0021889801018350).
[22] I.F. Bailey, Z. Krist. **218**(2) 84–95 (2003) (doi:10.1524/zkri.218.2.84.20671).
[23] S.C. Nam and P.E. Hockberger, Pflügers Archiv Eur. J. Phys. **420**(1) 106–108 (1992) (doi:10.1007/BF00378649).
[24] R.M. Ibberson, W.I.F. David and K.S. Knight, RAL-92-031, Rutherford Appleton Laboratory, Oxfordshire, UK (1992) (http://www.isis.rl.ac.uk/crystallography/hrpd).
[25] M.T.F. Telling and K.H. Anderson, Phys. Chem. Chem. Phys. **7** 1255–1261 (2005) (doi:10.1039/b413934h).
[26] A.P. Rollet and G. Vuillard, C. R. Acad. Sci. Paris. **243** 383–386 (1956).
[27] J.P. Chan and W.F. Giauque, J. Phys. Chem. **68**(10) 3053–3057 (1964) (doi:10.1021/j100792a055).
[28] J.E. Bertie and M.R. Shehata, J. Chem. Phys. **81**(1) 27–30 (1984) (doi:10.1063/1.447381).
[29] J.S. Loveday and R.J. Nelmes, in *Science and Technology of High Pressure: Proceedings of AIRAPT-17*, edited by M.H. Manghnani, W.J. Nellis and M.T. Nicol, (Universities Press, Hyderabad, India, 2000), pp. 133–136.
[30] A.D. Fortes, I.G. Wood, J.P. Brodholt *et al.*, Icarus **162**(1) 59–73 (2003) (doi:10.1016/S0019-1035(02)00073-8).
[31] A.D. Fortes, I.G. Wood, K.S. Knight *et al.*, J. Chem. Phys. **119**(20) 10806–10813 (2003) (doi:10.1063/1.1619371).
[32] E.L. Gromnitskaya, O.V. Stal'gorova, V.V. Brazhkin *et al.*, Phys. Rev. B **64** 094205 (2001) (doi:10.1103/PhysRevB.64.094205).
[33] J.S. Loveday and R.J. Nelmes, Phys. Rev. Lett. **83**(21) 4329–4332 (1999) (doi:10.1103/PhysRevLett.83.4329)
[34] A.C. Larsen and R.B. Von Dreele, General Structure Analysis System (GSAS). Los Alamos National Laboratory Report LAUR B6-748, Los Alamos, New Mexico (1988) (http://www.ncnr.nist.gov/xtal/software/gsas.html).

[35] A.Z. Kuznetsov, V. Dmitriev, L. Dubrovinsky *et al.*, Solid State Commun. **122**(3–4) 125–127 (2002) (doi:10.1016/S0038-1098(02)00112-6).
[36] R.A. Miller and D.E. Schuele, J. Phys. Chem. Solids **30** 589–600 (1969) (doi:10.1016/0022-3697(69)90014-6).
[37] Y.S. Touloukian, R.K. Kirby, R.E. Taylor *et al.*, in *Thermal Expansion, Metallic Elements and Alloys*, TPRC series on thermophysical properties of matter, volume 12, edited by S. Touloukian and C.Y. Ho, (Plenum, New York, 1975).
[38] D.L. Waldorf and G.A. Alers, J. Appl. Phys. **33**(11) 3266–3269 (1962) (doi:10.1063/1.1931149).

Appendix A

Pressure calibration using the equation of state of Pb

The Pb equation of state employed was derived from a synthesis of literature values for the ambient-pressure thermal expansivity, and ultrasonic determinations of the temperature dependence of K_0 and K_0' [35–38].

The pressure was determined using a Birch–Murnaghan equation of state,

$$P_{\mathrm{V,T}} = \frac{3}{2} K_{0,\mathrm{T}} (x^{7/3} - x^{5/3}) \cdot \left[1 + \frac{3}{4} (K'_{0,\mathrm{T}} - 4)(x^{2/3} - 1) \right]$$

where $x = V_{0,\mathrm{T}} / V_{\mathrm{P,T}}$; and the unit-cell volume, $V_{0,\mathrm{T}}$, the isothermal bulk modulus, $K_{0,\mathrm{T}}$, and its first pressure derivative, $K'_{0,\mathrm{T}}$, are found from temperature dependent polynomials;

$$V_{0,\mathrm{T}} = V_{0,0} + aT + bT^2, \quad \text{where } \mathrm{V}_{0,0} = 29.6496\,\text{Å}^3,\ a = 1.9301 \times 10^{-3}\,\text{Å}^3\,\mathrm{K}^{-1},$$
$$b = 9.9177 \times 10^{-7}\,\text{Å}^3\,\mathrm{K}^{-2}.$$
$$K_{0,\mathrm{T}} = K_{0,0} + cT + dT^2, \quad \text{where } K_{0,0} = 48.80\,\mathrm{GPa},\ c = 2.134 \times 10^{-2}\,\mathrm{GPa\,K}^{-1},$$
$$d = 6.762 \times 10^{-6}\,\mathrm{GPa\,K}^{-2}.$$
$$K'_{0,\mathrm{T}} = K'_{0,0} + eT, \quad \text{where } K'_{0,0} = 5.3944,\ e = 0.0011\,\mathrm{K}^{-1}$$

The estimated precision of these pressure determinations is ±0.1 GPa. In a few circumstances, where ice VIII has been observed, it has been possible to use an equation of state for ice VIII to cross-check the pressure, and the agreement has typically been better than 0.05 GPa.